Journal of Materials Chemistry C

Accepted Manuscript

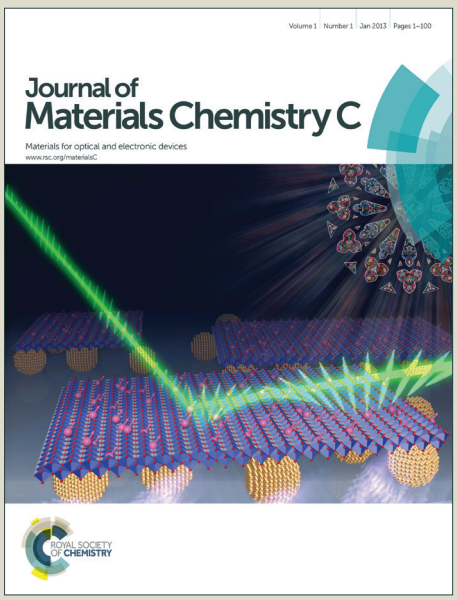

ROYAL SOCIETY OF CHEMISTRY

www.rsc.org/materialsC

Journal Name

RSCPublishing

ARTICLE

Structure and photoluminescence properties of novel Ca_2NaSiO_4F: Re (Re = Eu^{2+},Ce^{3+},Tb^{3+}) phosphor with energy transfer for white emitting LEDs

Cite this: DOI: 10.1039/xoxxoooooox

Received ooth January 2012,
Accepted ooth January 2012

DOI: 10.1039/xoxxoooooox

www.rsc.org/

Mengmeng Jiao,[a,b] Yongchao Jia,[a,b] Wei Lü,[a] Wenzhen Lv,[a,b] Qi Zhao,[a,b] Baiqi Shao,[a,b] Hongpeng You,*[a]

A series of Eu^{2+} and Ce^{3+}/Tb^{3+} doped Ca_2NaSiO_4F (CNSOF) phosphors have been synthesized and their structure and photoluminescence properties have been investigated in detail. Reviteld structure refinement indicates that the phosphors crystalized in orthorhombic system with space group of Pnma (no.62) and there are two kinds of cation sites for the doped ions to occupy forming emission centers. The CNSOF:Eu^{2+} and CNSOF:Ce^{3+} phosphors both have broad excitation bands, which match well with the commercial UV LED chips. The CNSOF:Eu^{2+} phosphor can have intense green emission with maximum at 530 nm under the irradiation of 380 nm, while the CNSOF:Ce^{3+} sample can emit intense blue light peaking at 470 nm at the excitation of 365 nm. By codoping the Tb^{3+} and Ce^{3+} ions into CNSOF host and varying their relative ratio, tunable blue-green colors are obtained due to efficient energy transfer from the Ce^{3+} to Tb^{3+} ions. Moreover, energy transfer mechanisms for the Eu^{2+} ions in CNSOF:Eu^{2+} and the Ce^{3+}→Tb^{3+} in CNSOF:Ce^{3+},Tb^{3+} both have been studied systematically.. Our investigation indicates that the CNSOF:Eu^{2+} and CNSOF:Ce^{3+},Tb^{3+} may be potential green and blue-green phosphors for UV WLEDs, respectively.

1. Introduction

In recent years, luminescent materials doped with lanthanide and transitional metal ions have arisen great interest due to their wide applications in light-emitting diodes (LEDs), field emission displays (FEDs), plasma display panels (PDPs), lasers and so on.[1-4] Among these applications, the white light emitting diodes (WLEDs) have been regarded as the next generation illumination due to their energy saving, environmental friendliness, high efficiency merits over the traditional incandescent and fluorescent lamps.[5,6] Since WLEDs fabricated with three (blue, green, red) LEDs need complicated technology and high expense,[6,7] the main approach to obtain WLEDs is the combination of blue or ultra violet LED with down converting phosphors, known as phosphor-converted WLEDs. Currently, commercial white LED is dominated by the blue InGaN chip and $Y_3Al_5O_{12}$:Ce^{3+}($YAG:Ce^{3+}$) phosphor. However, this kind of white LED suffers the problem of high correlated colour temperature (T_c > 4500 K) and low rending index (R_a < 80), which restrict their application in many fields such as general illumination and medical lighting etc.[8,9] To overcome the above disadvantage, white LEDs realized by UV LEDs coated with tricolour (blue, green, red) phosphors were employed. This kind of combination has great colour rendering index and easily controlled luminescence properties and are expected to dominate the market in the future.[10,11] Thus, it is of great importance to explore novel phosphors which can be excited by the UV LED chips.

The luminescence properties of lanthanide ions have been widely investigated and the rare earth ions were used as luminescent centres in most inorganic phosphors because of their abundant emission colour.[12-15] It is well known that the Eu^{2+} and Ce^{3+} ions can have broad excitation and emission bands with high efficiency due to their spin and orbit allowed 4f-5d electronic transitions.[16] Moreover, the emission colour of Eu^{2+} and Ce^{3+} ions in different hosts can change from blue to yellow (and even red) depending on different crystal field splitting resulted from their surrounding ligands.[17,18] In this case, the Eu^{2+} and Ce^{3+} activated phosphors have been widely synthesized and investigated. For example, Li et al. have synthesized the Eu^{2+} doped yellow emitting $Ba_{0.93}Eu_{0.07}Al_2O_4$ phosphor with low correlated colour temperature (CCT).[19] WonBin Im et al. have synthesized $Sr_{2.975-x}Ba_xCe_{0.025}AlO_4F$ green phosphor and $La_{1-x-0.025}Ce_{0.025}Sr_{2+x}Al_{1-x}Si_xO5$ yellow phosphor.[20,21] The Tb^{3+} ion is regard as promising green activator for showing sharp lines at 488, 543, and 582 nm due to the $^5D_4$-$^7F_6$, $^5D_4$-$^7F_5$, $^5D_4$-$^7F_4$ transition, respectively. However, to have intense Tb^{3+} emission in the phosphor,

sensitizers are needed since the f-f transitions of Tb^{3+} ion is spin-forbidden.[22,23]

The dicalcium sodium fluoride silicate Ca_2NaSiO_4F, which was first reported by Brosset in 1945, can be regarded as the sodium-rich end member of a series of solid-solution compound Ca_2SiO_4 $(CaO)_{1-x}$ $(NaF)_x$ in which x = 1. In 1997, Ő.Andaç et al reported its structure by investigating the single crystal X-ray diffraction data.[24] The refinement results of occupancy factors for Ca and Na indicate that the total ratio of them is slightly different from 2:1, and thus which may require vacancy on fluorine position. In 2008, Krüger and Kahlenberg reported a new monoclinic Ca_2NaSiO_4F and studied its structure.[25] However, the luminescence properties of rare earth ions in Ca_2NaSiO_4F have not been reported. In this paper, we studied the structure and luminescence properties of Eu^{2+}, Ce^{3+} and Tb^{3+} doped Ca_2NaSiO_4F phosphors. The CNSOF:Eu^{2+} and CNSOF:Ce^{3+} phosphors both can be efficiently excited by the UV light. The CNSOF:Eu^{2+} can have green emission under the irradiation of 380 nm, while the CNSOF:Ce^{3+} can emit intense blue light at the excitation of 365 nm. The luminescence properties and energy transfer mechanism of the Ce^{3+} and Tb^{3+} codoped samples have also been investigated in detail.

2. Experimental Section

2.1. Materials and synthesis

The phosphors with composition of CNSOF:$x$$Eu^{2+}$ (x = 0.002-0.03) and CNSOF:$y$$Ce^{3+}$,$z$$Tb^{3+}$ (y= 0-0.06, z = 0-0.18) were synthesized by conventional high temperature solid-state reaction. The $CaCO_3$ (A.R.), CaF_2 (A.R.), SiO_2 (A.R.), Na_2CO_3 (A.R.), Eu_2O_3 (99.99%), CeO_2 (99.99%), Tb_4O_7 (99.99%) were used as the starting materials and were weighed in a proper stoichiometric ratio with 10% excess of Na_2CO_3 using as flux. The mixtures were first mixed and grind in an agate mortar for 15 min, and then were sintered at 1100 ℃ for 3 h under a reductive atmosphere (20% H_2 + 80% N_2). Finally, the prepared phosphors were cooled to room temperature and reground for further measurements.

2.2. Measurements and Characterization

The Powder X-ray diffraction (XRD) data were obtained from D8 Focus diffractometer (Bruker) operating at 40 kV and 40 mA with Cu Kα radiation (λ = 1.5418 Å). The photoluminescence excitation (PLE) and photoluminescence (PL) measurements were performed on Hitachi F-4500 spectrophotometer equipped with a 150W Xenon lamp as the excitation source. The luminescence decay curves were obtained from a Lecroy Wave Runner 6100 Digital Oscilloscope (1 GHz) using a tunable laser (pulse width = 4 ns, gate = 50 ns) as the excitation. Photoluminescence quantum yields of the phosphors were determined on a quantum yield measurement system (C9920–02, Hamamatsu Photonics K.K., Japan). The emission spectra of the phosphors at different temperatures were performed on the Edinburgh Instrument FLS 920 spectrophotometer with the Advanced Research System Inc. as the temperature controlling system.

3. Results and Discussion

3.1 Phase formation and crystal characters

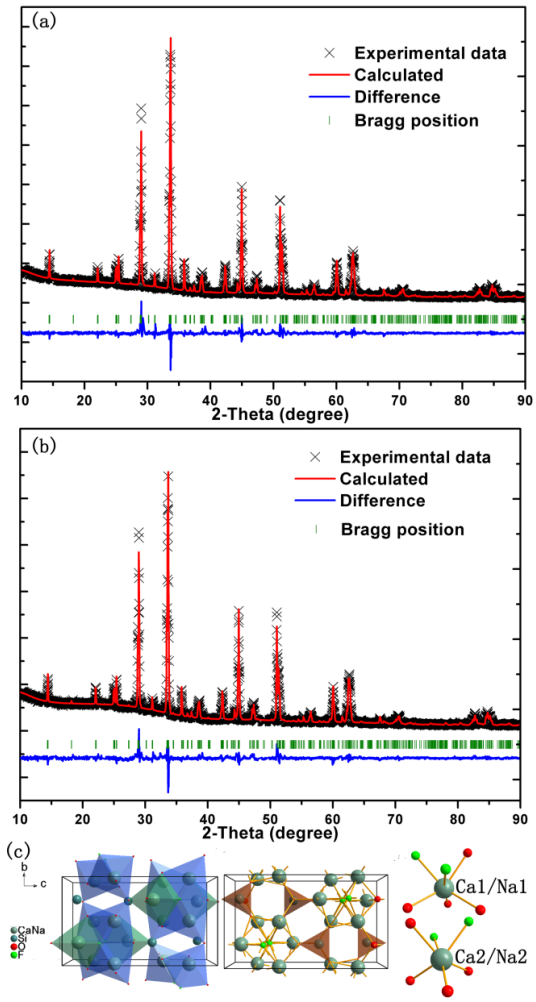

Figure 1. (a) Reviated structure pattern of CNSOF:0.02Eu^{2+} sample. (b) Reviated structure pattern of CNSOF:0.03Ce^{3+} sample. (c) Unit cell structure of CNSOF host and the coordination environment of the Ca^{2+} and Na^{+} ions.

To verify the crystal structure of the phosphor, Rietveld structure refinements of our typical prepared phosphors had been performed using the general structure analysis system (GSAS) program.[26] The refinement patterns of CNSOF:0.02Eu^{2+} and CNSOF:0.03Ce^{3+} samples are shown in Figure 1(a) and (b), while the final refinement parameters are shown in Table S1 and S2 (Supplementary information). In the refinement, the crystal structure data (ISCD# 59273) reported by Ő.Andaç et al in 1997 were used as initial parameters. The phosphors crystalize in the orthorhombic system with space group being Pnma (no.62). For the CNSOF:0.02Eu^{2+} phosphor, the cell parameters are calculated to be a = 5.3387, b = 7.1253 Å, c = 12.4407 Å, V = 473.242Å^3, Z = 4, and the reliability factors are χ^2 = 3.849, R_{wp} = 7.06%, R_p = 5.15%. For the

CNSOF:0.03Ce^{3+} sample, the cell parameters are determined to be a = 5.3371, b = 7.1273 Å, c = 12.4374 Å, V = 473.101Å^3, Z = 4, and the reliability factors are χ^2 = 3.274, R_{wp} = 6.57%, R_p = 4.90%. The cell parameters of the two samples are similar to that of the host reported earlier[24] and the slight difference can be ascribed to the doping of rare earth ions. The reliability factors for the two samples indicate that the atom positions, fraction factors, and temperature factors of the samples all well satisfy the reflection conditions. The typical XRD patterns for our prepared samples shown in Figure S1 (Supplementary information) together with the standard data (PDF# 87-0439) can also validate the phase purity of the obtained phosphors. Figure 1(c) depicts the unit cell structure of CNSOF along the a-direction and the coordination environment of the cation sites. In the host, there are two kinds of cation sites named M1 and M2 here and equal numbers of isolated $[SiO_4]^{4-}$ and F^- anions. The two cation sites are both occupied by Ca and Na ions, moreover, the Ca1/Na1 and Ca2/Na2 are coordinated by four oxygen atoms and two fluorine atoms forming distorted octahedrons. The Si ions are coordinated by four oxygen atoms in a very regular tetrahedral. Each oxygen atom is coordinated by three Ca/Na atoms in addition to Si in a distorted tetrahedral, while the F atom is surround by six Ca/Na forming octahedron.

3.2 Photoluminescence properties of CNSOF:Eu^{2+} phosphor

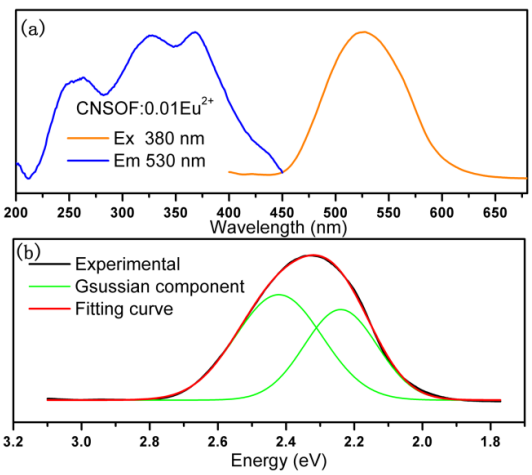

Figure 2. (a) PL and PLE spectra of CNSOF:0.01Eu^{2+} sample. (b) Emission spectrum of CNSOF:0.01Eu^{2+} and its Gaussian components on an energy scale.

Figure 2(a) shows the photoluminescence (PL) and photoluminescence excitation (PLE) spectra of CNSOF:0.01Eu^{2+} phosphor. The excitation spectrum monitored at 530 nm exhibits a broad excitation band ranging from 200 to 450 nm, which matches well with the commercial n-UV LED chips (380-420nm). Under the excitation of 380 nm, the phosphor shows a strong green emission ranging from 450 to 600 nm with maximum at 530 nm due to the electron transition from the $4f^65d^1$ excited state to the $4f^7$ ground state. As shown in Figure 2(b) the broad emission band can be well decomposed into two separated Gaussian components on an energy level, which can be ascribed to the two different Eu^{2+} emission centres. This luminescence property is consistent with the structure analysis of the phosphor discussed previously. The PL and PLE spectra of CNSOF:0.01Eu^{2+} phosphor indicate that this obtained sample has potential value as the n-UV excited green phosphor for WLEDs.

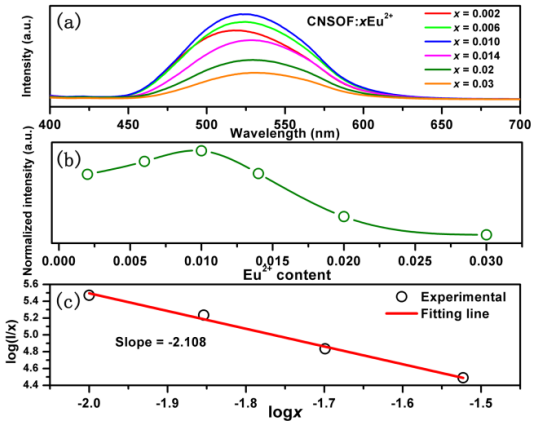

Figure 3. (a) Emission spectra of CNSOF:xEu^{2+} (x = 0.002, 0.006, 0.01, 0.014, 0.02, 0.03) samples under 380 nm excitation. (b) Variation of emission intensity as a function of doped Eu^{2+} content for CNSOF:xEu^{2+} phosphors. (c) Dependence of log(I/x) on log$x$ in CNSOF:xEu^{2+} samples.

To investigate the effect of concentration on the luminescence properties of the samples, a series of CNSOF:xEu^{2+} (x = 0.002-0.03) was prepared. Figure 3(a) depicts the emission spectra of the phosphors with different Eu^{2+} content under the 380 nm irradiation. With the increasing of Eu^{2+} content, one can see that the emission peak wavelength has a red shift, which can be explained by the energy transfer to Eu^{2+} ions emitting at longer wavelength.[27,28] The emission intensity of the phosphor first increases gradually to a maximum at x = 0.01 and then decreases due to the concentration quenching of the Eu^{2+} ions. This variation of emission intensity has also been shown in Figure 3(b). Moreover, the emission spectrum of CNSOF:0.01Eu^{2+} phosphor was compared with the commercial green $Y_3(Al,Ga)_5O_{12}:Ce^{3+}$ phosphor at 380 nm irradiation (Figure S2, Supplementary Information). The integral emission intensity of our prepared phosphor was determined to be 1.04 times of the $Y_3(Al,Ga)_5O_{12}:Ce^{3+}$ phosphor under the same condition.

According to Dexter's energy transfer theory, the concentration quenching is mainly caused by the nonradiative energy migration among the Eu^{2+} ions at high concentration. The critical distance between the doped ions can be calculated by the concentration quenching method using the following equation:[29]

$$R_C \approx 2\left[\frac{3V}{4\pi x_C N}\right]^{1/3} \quad (1)$$

where N represents the number of sites that the Eu^{2+} ion can occupy in the host, x_C is the critical concentration, and V stands for the unit cell volume. Under the present condition, x_C = 0.01, $N = Z \times 2 = 8$, V= 474.05. Thus, the R_C was determined to be 22.45 Å, which is much larger than 5 Å. It is well accepted that

the nonradiative energy migration is usually caused by exchange interaction or multipole-multipole interaction.[30] Since the former comes into effect only when $R_C < 5$Å, the multipole-multipole interaction is considered to be responsible for the energy migration. According to the report of Van Uiter,[31] the emission intensity (I) per activator can be given by the equation,

$$I/x = k\left[1 + \beta(x)^{\theta/3}\right]^{-1} \qquad (2)$$

where I stands for the luminescence intensity, k and β are constant for a given host under the same condition; x represents the Eu^{2+} doping content; θ = 6, 8, and 10 correspond for the dipole-dipole, dipole-quadrupole, and quadrupole-quadrupole interaction, respectively. After taking logarithm, the $\log(I/x)$ was plotted as a function of $\log(x)$ and was shown in Figure 3(c). The slope of the fitting line which equals to $\theta/3$ was calculated to be -2.108, and thus the θ was determined to be 6.324. This result indicates that the concentration quenching mechanism is dominated by dipole-dipole interaction.

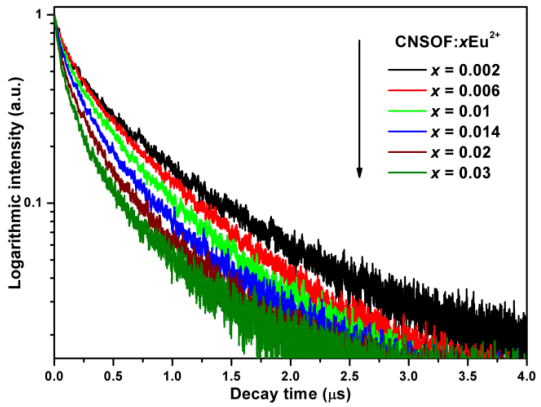

Figure 4. Decay curves for Eu^{2+} emission in CNSOF:xEu^{2+} samples (excited at 330 nm, monitored at 530 nm).

Figure 4 demonstrates the luminescence decay curves of the CNSOF:xEu^{2+} phosphors monitored at 530 nm with the irradiation of 330 nm. It is obvious that all the decay curves deviate from the single exponential function, which is also consistent with the structure analysis that there are two Eu^{2+} emitting centres in the phosphor. The increment of Eu^{2+} content will enhance this deviation, which can be ascribed to the nonradiative energy migration among the activators. In addition, the average lifetime of the Eu^{2+} ions in the CNSOF:xEu^{2+} phosphor was calculated by using the equation:

$$\tau_{avg} = \int_0^\infty tI(t)\,dt / \int_0^\infty I(t)dt \qquad (3)$$

where $I(t)$ stands for the emission intensity of Eu^{2+} at time t. The decay times for Eu^{2+} ions in CNSOF:xEu^{2+} phosphors with x = 0.002, 0.006, 0.010, 0.014, 0.02, and 0.03 were determined to be 583, 493, 428, 379, 322, and 294 ns, respectively. The decrement of the Eu^{2+} lifetime was also caused by the nonradiatiove energy migration among the Eu^{2+} ions.

3.3 Luminescence properties of CNSOF:Ce^{3+}/Tb^{3+} phosphors

Figure 5 shows the excitation and emission spectra of CNSOF:0.05Tb^{3+} phosphor. The excitation spectrum monitored at 542 nm consists of a broadband with maximum at 260 nm and several peaks in the range of 300 to 500 nm (enlarged in the inset of Figure 5). The broadband excitation is caused by the f-d electron transition of the Tb^{3+} ions, while the excitation peaks can be ascribed to the f-f transition. At the excitation of 260 nm, the emission spectrum includes two sets of emission peaks. The blue emissions with peaks at 380, 418, and 439 nm are due to the $^5D_3$-^7F_J (J = 6, 5, 4) transitions, whereas the green emission peaks at 487, 542, 586, and 620 nm are due to the $^5D_4$-^7F_J (J = 6, 5, 4, 3) transitions. Since the energy difference between the $^5D_3$ and $^5D_4$ energy level is similar to that between $^7F_0$ and $^7F_6$, the cross relaxation which can be demonstrated as $^5D_3$ (Tb^{3+}) + $^7F_6$ (Tb^{3+}) →$^5D_4$ (Tb^{3+}) + $^7F_0$ (Tb^{3+}) will occur at high Tb^{3+} content.[32,33] Thus, with the increment of Tb^{3+} content, the blue emission will be quenched while the green emission will be populated. For the CNSOF:0.05Tb^{3+} content, the emission is dominated by the green emission.

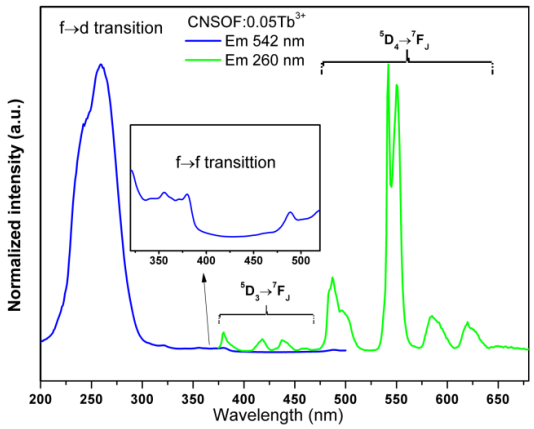

Figure 5. PLE and PL spectra of CNSOF:0.05Tb^{3+} phosphor. The inset shows the enlarged excitation spectrum in the range from 320 to 520 nm.

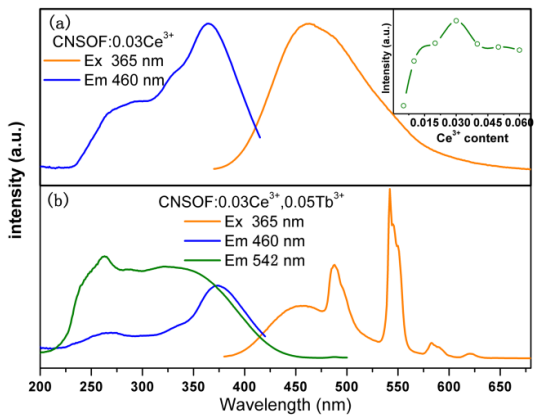

Figure 6. PLE and PL spectra of (a) CNSOF:0.03Ce^{3+} and (b) CNSOF:0.03Ce^{3+},0.05Tb^{3+} phosphors. The inset of Figure 6 (a) depicts the dependence of CNSOF:yCe^{3+} emission intensity on the Ce^{3+} content.

The excitation and emission spectra of the CNSOF:0.03Ce^{3+} phosphor have been depicted in Figure 6(a). Monitored at 460 nm, the phosphor shows a broad excitation band ranging from 240 to 400 nm with maximum at 365 nm, indicating that this phosphor can be excited efficiently by the UV light. Under the irradiation of 365 nm, the phosphor can emit intense blue light in the range of 400 to 575 nm with peak wavelength at 460 nm. The inset of Figure 6 (a) shows the

relative emission intensity of CNSOF:yCe^{3+} phosphors with different Ce^{3+} contents. It can be seen that the emission intensity increased gradually to a maximum at y = 0.03, beyond which the intensity decreased gradually due to the concentration quenching. The energy migration among the Ce^{3+} ions at high concentration is responsible for this phenomenon. The emission spectrum of CNSOF:0.03Ce^{3+} phosphor has an overlap with the excitation peak of the Tb^{3+} ions at 487 nm due to the $^7F_6$-$^5D_4$ electronic transition, and thus the energy transfer from the Ce^{3+} to Tb^{3+} ions can be expected. Figure 6 (b) shows the PL and PLE spectra of CNSOF:0.03Ce^{3+},0.05Tb^{3+} phosphor. At the excitation of 365 nm, the phosphor shows both intense blue emission of the Ce^{3+} ions and green emission of the Tb^{3+} ions. Monitored at 542 nm which is the typical emission of the Tb^{3+} ions, the excitation spectrum shows a broad band consisting of both the f-d transition of the Tb^{3+} and the Ce^{3+} ions. The excitation monitored at 460 nm is not very consistent with that of the Ce^{3+} singly doped phosphor. This phenomenon may be explained by that the Ce^{3+} ions at different sites have different contribution to energy transfer process from the Ce^{3+} to Tb^{3+} ions.

To further validate the presence of the energy transfer process, phosphors with varied Ce^{3+} or Tb^{3+} content were prepared and their emission spectra were shown in Figure 7(a) and (b). For CNSOF:0.03Ce^{3+},zTb^{3+} (z = 0-0.18) phosphors, the emission intensity of the Ce^{3+} ions decreased monotonously with the increasing of Tb^{3+} content, while the emission intensity of Tb^{3+} first increased to a maximum at y = 0.15 and then decreased due to the concentration quenching. Figure 7(b) depicts the emission spectra of CNSOF:yCe^{3+},0.15Tb^{3+} phosphors. It is obvious that the emission of the Tb^{3+} singly doped phosphor is pretty weak compared with the Ce^{3+} and Tb^{3+} codoped samples since the f-f transition of Tb^{3+} is spin forbidden. The doping of Ce^{3+} dramatically enhanced the emission intensity of the Tb^{3+} ions. Moreover, although the content of the Tb^{3+} ion is fixed, the emission intensity of the Tb^{3+} firstly increases with the increasing of Ce^{3+} doping concentration, which further confirming the presence of energy transfer from the Ce^{3+} to Tb^{3+} ions. When the concentration of the Ce^{3+} ions is beyond 0.04, the emission intensity of the Tb^{3+} ions starts to decrease due to concentration quenching. The optimum Ce^{3+} concentration is 0.04 in CNSOF:yCe^{3+},0.15Tb^{3+} phosphors, which is different from that in CNSOF:yCe^{3+} phosphors. This can be ascribed to the influence of the Tb^{3+} ions on the emission of the Ce^{3+} ions. The comparison of the emission spectra between the CNSOF:0.04Ce^{3+},0.15Tb^{3+} phosphor and the commercial green $Y_3(Al,Ga)_5O_{12}$:Ce^{3+} phosphor was shown in Figure S3 (Supplementary Information). Under 365 nm irradiation, the integral emission intensity of our prepared phosphor was 1.13 times stronger than the $Y_3(Al,Ga)_5O_{12}$:Ce^{3+} phosphor. Moreover, the emission intensity of our obtained phosphor can be improved by optimum the experimental condition.

The luminescence intensity of most phosphors will decrease with the increment of temperature due to the temperature quenching. Since the LEDs operate at temperature of about 150 ℃,[34] it is important to find phosphors with good thermal stability. Figure 8 shows the relative intensity of typical CNSOF:0.03Ce^{3+} and CNSOF:0.03Ce^{3+},0.08Tb^{3+} phosphors at different temperatures. It can be seen that the emission intensity of the two phosphors both decrease monotonously with the temperature increased from 298 to 473 K. At 423 K, the emission intensity of CNSOF:0.03Ce^{3+} and CNSOF:0.03Ce^{3+},0.08Tb^{3+} decrease to 65.5% and 60.0% of their value at 298K, respectively. The quenching temperature T_{50}, defined as the temperature at which the emission intensity is 50% of its original value, were determined to be 456 and 464 K for CNSOF:0.03Ce^{3+}, CNOSF:0.03Ce^{3+},0.07Tb^{3+} phosphors, respectively. The temperature quenching of the phosphors is due to the temperature dependent phonon interaction. At high temperature, the electrons at lowest excited state C can be easily activated, and then released through the crossing point E between the excited state and the ground state in configurational coordinate diagram. Thus, decrement of the emission intensity occurs with temperature incrasing.[35,36]

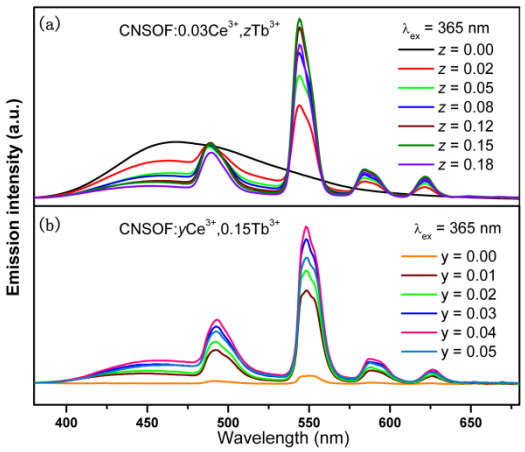

Figure 7. Emission spectra of (a) CNSOF:0.03Ce^{3+},zTb^{3+} (z = 0–0.18) and (b) CNSOF:yCe^{3+},0.15Tb^{3+} (y = 0–0.05) phosphors.

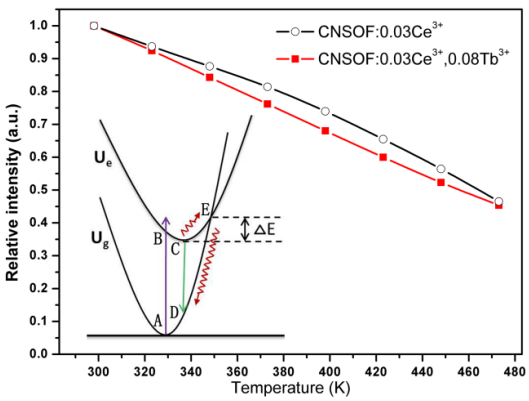

Figure 8. Normalized emission intensity of CNSOF:0.03Ce^{3+} and CNSOF:0.03Ce^{3+},0.08Tb^{3+} phosphors at different temperatures, together with the configurational coordinate diagram for the explanation of thermal quenching.

3.4 Mechanism of Energy transfer from Ce^{3+} to Tb^{3+}

To study the luminescence dynamic of the samples, decay curves of the CNSOF:0.03Ce^{3+},zTb^{3+} phosphors with z varying from 0 to 0.18 are measured and depicted in Figure 9. It can be clearly seen that the doping of the Tb^{3+} ions modified the luminescence dynamic of the Ce^{3+} ions. All the decay curves are deviate from the single exponential function. The deviation becomes more obvious with the increasing of the Tb^{3+} content due to the non-radiative energy transfer process from the Ce^{3+} to Tb^{3+} ions. By using the equation (3), the average lifetimes were calculated to be 63.2, 58.9, 54.7, 52.8, 50.9, 45.1, and 43.2 ns for Ce^{3+} ions in CNSOF:0.03Ce^{3+},zTb^{3+} samples with z being 0.00, 0.02, 0.05, 0.08, 0.12, 0.15 and 0.18, respectively.

The energy transfer efficiency from Ce^{3+} to Tb^{3+} ions was also calculated by equation:[37]

$$\eta_T = 1 - \tau_S/\tau_{S0} \quad (4)$$

where τ_S and τ_{S0} are emission intensity of phosphors with and without the presence of the Tb^{3+} ions. The lifetimes and energy transfer efficiencies were plotted as the function of Tb^{3+} content and were shown in Figure S4 (Supplementary Information). With the increment of the Tb^{3+} content, the lifetime of the Ce^{3+} ions decreased gradually from 63.0 to 43.2 ns, while the efficiency of the energy transfer process from the Ce^{3+} to Tb^{3+} ions was increased monotonously.

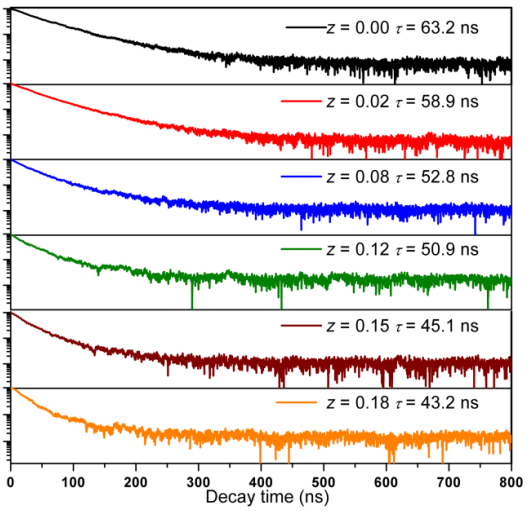

Figure 9. Decay curves for Ce^{3+} emission in CNSOF:0.03Ce^{3+},zTb^{3+} phosphors with different Tb^{3+} content (excited at 330 nm, monitored at 480 nm).

To analyze the mechanism of the energy transfer from the Ce^{3+} to Tb^{3+} ions, Inokuti−Hirayama model was employed.[38] It has been known that if the donors and acceptors in the host are distributed uniformly in the host, the energy migration process can be negligible compared to the energy transfer between donors and acceptors. The normalized intensity of the Ce^{3+} fluoresce with the presence of the Tb^{3+} ions can be written as

$$I_D(t) = I_{D0}(t)f(t) \quad (5)$$

where $I_{D0}(t)$ is the normalized decay function of Ce^{3+} ions in the host without the Tb^{3+} ions, the $f(t)$ function characterizes the energy loss of excited donors due to one-way energy transfer to the acceptors. If the energy transfer rate between a donor and an acceptor is inversely proportional to the distance, according to the I−H formula, we can get

$$f(t) = exp\left[-\frac{4}{3}\pi\Gamma\left(1-\frac{3}{m}\right)n_A\alpha^{3/m}t^{3/m}\right] \quad (6)$$

in which m = 6, 8, and 10 corresponds for the dipole-dipole, dipole-quadrupole, and quadrupole-quadrupole interaction, respectively; α is a rate constant represents for the energy transfer; n_A stands for the number of activator ions per unit volume. After modifying the equation (5) and (6), we can get a liner relation between $\log\{\ln[I_{D0}(t)/I_D(t)]\}$ and $\log(t)$ with a slope being $m/3$. To get an accurate value of m, the $\log\{\ln[I_{D0}(t)/I_D(t)]\}$ was plotted as a function of $\log(t)$ for three typical phosphors, as shown in Figure10. From the slope values of the fitting lines, the m were determined to be 8.13, 7.89, and 8.04 for the CNSOF:0.03Ce^{3+},zTb^{3+} samples with z being 0.05, 0.12, 0.18. Thus, the average value of m which is nearly consistent with 8 indicates that the dipole-quadrupole interaction is responsible for the energy transfer from the Ce^{3+} to Tb^{3+} ions.

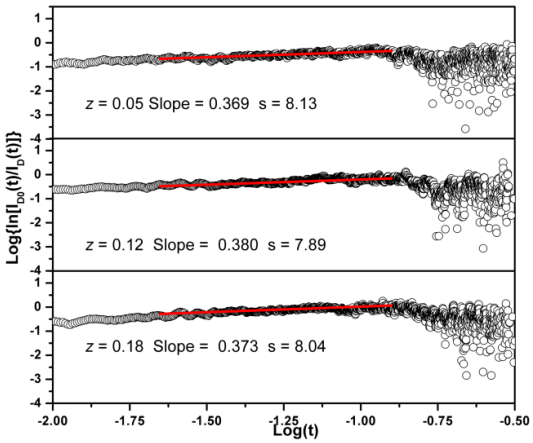

Figure 10. Dependence of $\log\{\ln[I_{D0}(t)/I_D(t)]\}$ on log(t) for CNSOF:0.03Ce^{3+},zTb^{3+} (z = 0.05, 0.12, 0.18) phosphors.

3.5 CIE coordinates and quantum efficiencies of prepared phosphors

Table 1. CIE coordinates and quantum efficiencies of CNSOF:0.01Eu^{2+} and CNSOF:0.03Ce^{3+},zTb^{3+} phosphors

Sample	CIE coordinates (x, y)	Quantum efficiency
CNSOF:0.01Eu^{2+}	(0.263, 0.567)	26.7%
CNSOF:0.03Ce^{3+}	(0.184, 0.257)	37.4%
CNSOF:0.03Ce^{3+},0.02Tb^{3+}	(0.223, 0.338)	34.2%
CNSOF:0.03Ce^{3+},0.05Tb^{3+}	(0.251, 0.405)	33.2%
CNSOF:0.03Ce^{3+},0.08Tb^{3+}	(0.260, 0.424)	33.7%
CNSOF:0.03Ce^{3+},0.12Tb^{3+}	(0.277, 0.457)	34.7%
CNSOF:0.03Ce^{3+},0.15Tb^{3+}	(0.281, 0.463)	39.3%
CNSOF:0.03Ce^{3+},0.18Tb^{3+}	(0.289, 0.470)	30.3%
CNSOF:0.15Tb^{3+}	(0.297, 0.502)	11.9%
CNSOF:0.01Ce^{3+},0.15Tb^{3+}	(0.287, 0.471)	25.6%
CNSOF:0.02Ce^{3+},0.15Tb^{3+}	(0.284, 0.467)	28.3%
CNSOF:0.04Ce^{3+},0.15Tb^{3+}	(0.275, 0.439)	33.7%
CNSOF:0.05Ce^{3+},0.15Tb^{3+}	(0.269, 0.432)	31.2%

The CIE coordinates of the CNSOF:0.01Eu^{2+} and CNSOF:0.03Ce^{3+},zTb^{3+} samples with different doping contents of the Tb^{3+} ions have been obtained by integrating their corresponding photoluminescence emission spectra. Table 1 and Figure 11 have shown the chromaticity coordinates and CIE chromaticity diagram of the samples, respectively. The CNSOF:0.01Eu^{2+} has a green emission with coordinates being (0.263, 0.567). For the CNSOF:0.03Ce^{3+},zTb^{3+} phosphors, tunable blue-green emission with CIE coordinates varying from (0.184, 0.257) to (0.289, 0.470) can be easily obtained by changing the doping content of the Tb^{3+} ion. In order to have a more intuitive express on the emission colors of our prepared samples, the digital photographs taken under a 365 nm UV lamps were also shown in Figure 11. Quantum efficiency as an important parameter for phosphors was also measured and

listed in Table 1. The CNSOF:0.01Eu^{2+} sample has a quantum efficiency of being 26.7%, while the quantum efficiency of CNSOF:0.03Ce^{3+} phosphor can reach 37.4%. Moreover, by optimizing the experimental conditions and the compositions of the phosphors, the quantum efficiency can be improved. The photoluminescence properties of the prepared phosphors indicate that the CNSOF:Eu^{2+} and CNSOF:Ce^{3+},Tb^{3+} samples may have potential value for UV WLEDs.

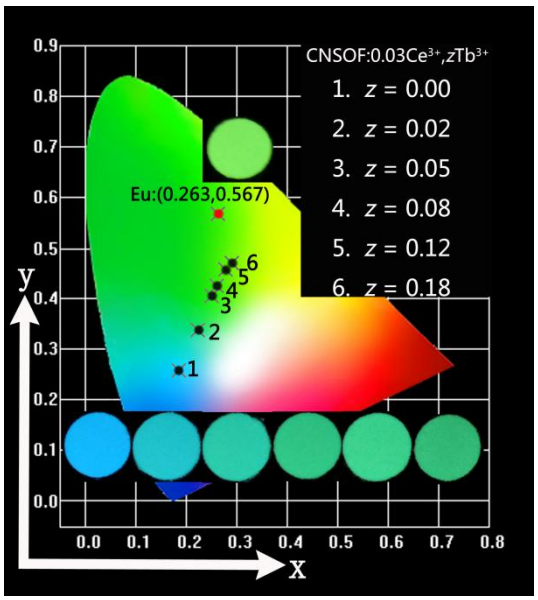

Figure 11. The CIE coordinate diagram for typical CNSOF:0.01Eu^{2+} and CNSOF:0.03Ce^{3+},zTb^{3+} (z = 0.00, 0.02, 0.05, 0.08, 0.12, 0.18) phosphors together with their photographs under 365 nm UV lamp.

Conclusions

In summary, a series of CNSOF:Eu^{2+} and CNSOF:Ce^{3+},Tb^{3+} phosphors have been synthesized by traditional high temperature solid state reaction. The phosphors crystalized in orthorhombic system and the doped rare earth ions in the phosphor are coordinated by four oxygen atoms and two fluorine atoms in two different ways. The CNSOF:Eu^{2+} phosphor can be efficiently excited by the light in the range from 200 to 430 nm and emit intense green light peaking at 530 nm. The energy migration mechanism for the Eu^{2+} ions was demonstrated to be dipole-dipole interaction. The CNSOF:Ce^{3+} phosphor can have intense blue emission with maximum at 470 nm under the 365 nm irradiation. By codoping Ce^{3+} and Tb^{3+} ions into the host, tunable blue-green colors are obtained. The dipole-quardrupole interaction was determined to be responsible for the energy transfer from the Ce^{3+} to Tb^{3+} ions. Moreover, the emission intensity of CNSOF:Ce^{3+} and CNSOF:Ce^{3+},Tb^{3+} phosphors at different temperatures was investigated. The luminescence properties of our prepared samples indicate that the CNSOF:Eu^{2+} might be potential green phosphor for NUV WLEDs, while the CNSOF:Ce^{3+},Tb^{3+} may have potential value as blue-green phosphor for UV WLEDs.

Acknowledgements

This work is financially supported by the National Basic Research Program of China (973 Program, grant no 2014CB6438003), and the National Natural Science Foundation of China (Grant Nos. 21271167 and 11304309) and the Fund for Creative Research Groups (Grant No. 21221061).

Notes and references

[a] State Key Laboratory of Rare Earth Resource Utilization, Changchun Institute of Applied Chemistry, Chinese Academy of Sciences, Changchun 130022, P. R. China.
[b] University of the Chinese Academy of Sciences, Beijing 100049, P. R. China.

Electronic Supplementary Information (ESI) available: [details of any supplementary information available should be included here]. See DOI: 10.1039/b000000x/

1 H. Daicho, T. Iwasaki, K. Enomoto, Y. Sasaki, Y. Maeno, Y. Shinomiya, S. Aoyagi, E. Nishibori, M. Sakata and H. Sawa, *Nat. Commun.*, 2012, **3**, 1132.
2 N. Hirosaki, R.-J. Xie, K. Inoue, T. Sekiguchi, B. Dierre and K. Tamura, *Appl. Phys. Lett.*, 2007, **91**, 061101.
3 C. Liu, S. Zhang, Z. Liu, H. Liang, S. Sun, and Y. Tao, *J. Mater. Chem. C*, 2013, **1**, 1305.
4 C.-C. Wu, K.-B. Chen, C.-S. Lee, T.-M. Chen and B.-M. Cheng, *Chem. Mater.*, 2007, **19**, 3278.
5 C. C. Lin and R.-S. Liu, *J. Phys. Chem. Lett.*, 2011, **2**, 1268.
6 S. Ye, F. Xiao, Y. X. Pan, Y. Y. Ma and Q. Y. Zhang, *Matet. Sci. Eng., R*, 2010, **71**, 1.
7 M.S. Shur, A. Zukauskas, *Proc. IEEE.*, 2005, **93**, 1691.
8 A. A. Setlur, W. J. Heward, Y. Gao, A. M. Srivastava, R. G. Chandran and M. V. Shankar, *Chem. Mater.* 2006, **18**, 3314.
9 Y. Liu, X. Zhang, Z. Hao, X. Wang and J. Zhang, *J. Mater. Chem.*, 2011, **21**, 6354.
10 Z. Xia and R.-S. Liu, *J. Phys. Chem. C*, 2012, **116**, 15604.
11 A. Katelnikovas, J. Plewa, S. Sakirzanovas, D. Dutczak, D. Enseling, F. Baur, H. Winkler, A. Kareivab and T. Jüstel, *J. Mater. Chem.*, 2012, **22**, 22126.
12 L. Wu, Y Zhang, M. Gui, P. Lu, L. Zhao, S. Tian, Y. Konga and J. Xu, *J. Mater. Chem.*, 2012, **22**, 6463.
13 S. Zhang, H. Liang and C. Liu, *J. Phys. Chem. C*, 2013, **117**, 2216.
14 D. Kang, H. S. Yoo, S. H. Jung, H. Kim and D. Y. Jeon, *J. Phys. Chem. C*, 2011, **115**, 24334.
15 G. Zhu, S. Xin, Y. Wen, Q. Wang, M. Que and Y. Wang. *RSC Adv.*, 2013, **3**, 9311.
16 D. Jia, R. S. Meltzer and W. M. Yen, *Appl. Phys. Lett.*, 2002, **80**, 1535.
17 K. A. Denault, Z. Chenga, J. Brgocha, S. P. DenBaarsab and R. Seshadri, *J. Mater. Chem. C.*, 2013, **1**, 7339.
18 G. Zhang, J. Wang, Y. Chen and Q. Su, *Opt. Lett.*, 2010, **35**, 2382.
19 X. Li, J. D. Budai, F. Liu, J. Y. Howe, J. Zhang, X.-J. Wang, Z. Gu, C. Sun, R. S. Meltzer and Z. Pan, *Light: Science & Applications*, 2013, **2**, e50.
20 W. B. Im, S. Brinkley, J. Hu, A. Mikhailovsky, S. P. DenBaars and R. Seshadri, *Chem. Mater.*, 2010, **22**, 2842.
21 W. B. Im, N. N. Fellows, S. P. DenBaars and R. Seshadri, *J. Mater. Chem.*, 2009, **19**, 1325.
22 M. Jiao, N. Guo, W. Lü, Y. Jia, W. Lv, Q. Zhao, B. Shao, H. You, *Inorg. Chem.*, 2013, **52**, 10340.

23 N. Guo, Y. Song, H. You, G. Jia, M. Yang, K. Liu, Y. Zheng, Y. Huang and H. Zhang, *Eur. J. Inorg. Chem.*, 2010, 4636.
24 Ő. Andaç, F. P. Glasser and R. A. Howie, *Acta Cryst.*, 1997. **C53**, 831.
25 H. Krüger and V. Kahlenberg, *Z. Kristallogr.*, 2008, **223**, 382.
26 A. C. Larson, R. B. Von Dreele, *Los Alamos Natl. Lab., [Rep.] LAUR.*, 1994, pp, 1-221.
27 V. Bachmann, C. Ronda, O. Oeckler, W. Schnick and A. Meijerink, *Chem. Mater.*, 2009, **21**, 316.
28 X.-M. Wang, X. Zhang, S. Ye and X.-P. Jing, *Dalton Trans.*, 2013, **42**, 5167.
29 G. Blasse, *Philips Res. Rep.*, 1969, **24**, 131.
30 D. L. Dexter, *J. Chem. Phys.*, 1953, **21**, 836.
31 L. G. Van Uitert, *J. Lumin.*, 1971, **4**, 1.
32 H. You, X. Wu, H. Cui and G. Hong, *J. Lumin.*, 2003. **104**. 223.
33 Y. Song, N. Guo and H. You, *Eur. J. Inorg. Chem.*, 2011, 2327.
34 M. Krings, G. Montana, R. Dronskowski and C. Wickleder, *Chem. Mater.*, 2011, **23**, 1694.
35 W. Lv, Y. Jia, Q. Zhao, M. Jiao, B. Shao, W. Lü and H. You, *Adv. Opt. Mater.*, 2014, **2**, 183.
36 G. Blasse, *J. Chem. Phys.*, 1968, **48,** 3108.
37 P. Paulose, G. Jose, V. Thomas, N. Unnikrishnan and M. Warrier, *J. Phys. Chem. Solids*, 2003, **64**, 841.
38 M. Inokuti and F. Hirayama, *J. Chem. Phys.*, 1965, **43**, 1978.

Structure and photoluminescence properties of novel Ca_2NaSiO_4F: Re (Re = Eu^{2+},Ce^{3+},Tb^{3+}) phosphor with energy transfer for white emitting LEDs

Mengmeng Jiao, Yongchao Jia, Wei Lü, Wenzhen Lv , Qi Zhao, Baiqi Shao, Hongpeng You

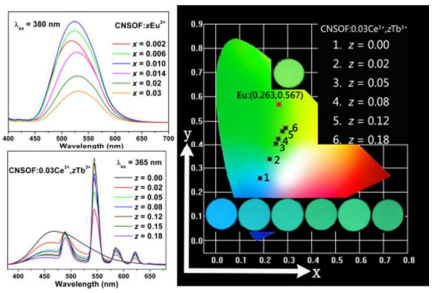

The Eu^{2+}, Ce^{3+} and Tb^{3+} doped Ca_2NaSiO_4F phosphors was prepared and their luminescence properties have been investigated systematically.